Characteristics of MHD Instabilities Limiting Beta Value in LHD

S.Sakakibara[1,2], K.Y.Watanabe[1], Y.Takemura[1], M.Okamoto[3], S.Ohdachi[1,2], Y.Suzuki[1,2], Y.Narushima[1,2], K.Ida[1,2], M.Yoshinuma[1], K.Tanaka[1], T.Tokuzawa[1], I.Yamada[1,2], H.Yamada[1,2], Y. Takeiri[1,2], and LHD Experiment Group[1]

[1]National Institute for Fusion Science, Toki 509-5292, Japan

[2]SOKENDAI (The Graduate University for Advanced Studies), Toki 509-5292, Japan

[3]Ishikawa National College of Technology, Ishikawa 929-0392, Japan

E-mail contact of main author: sakakibara.satoru@lhd.nifs.ac.jp

Abstract. Effects of low-*n* MHD instabilities on plasma performance have been assessed in the regime where an achieved beta value is limited by instabilities. The unstable regime of an ideal interchange mode is characterized by enhanced magnetic hill and reduced magnetic shear. Experiments have clarified that (i) low-*n* modes are significantly destabilized in the ideal-unstable configurations and lead to degradation of central beta by at most 60%, and (ii) the degree of their damages strongly depends on the mode rotation velocity. The occurrence of the minor collapse is independent of an existence of an error field.

1. Introduction

Suppression of magneto-hydrodynamic (MHD) instabilities is one of key subjects to be solved for realizing production of high-beta plasma in magnetic confinement systems. In tokamaks and RFPs, MHD instabilities driven by plasma current and/or plasma pressure obviously degrade plasma confinement and limit achieved beta value, and techniques for controlling them has been investigated for a long time. The plasma rotation control is one of candidates for the mode stabilization because experiments show that MHD modes such as tearing, external kink and so on abruptly grow and lead to major disruption after the mode rotation breaking. The rotation of the tearing mode is decelerated and stopped by the error field, and it leads to major disruption as a “locked mode” [1,2]. The restive wall mode, which is the instability to be suppressed for sustainment of high-beta plasma, can be suppressed by the plasma rotation [3]. Thus, the plasma flow driving the mode rotation is a key for stabilization of the modes, and effects of the toroidal flow driven by neutral

beams and rotating magnetic perturbations on the mode stabilization has been verified through a variety of experiments in tokamaks [3].

In heliotron configurations, interchange instability is one of the major concerns for high beta plasma production because of magnetic hill at the plasma where strong pressure gradient is formed with an increase in beta value. The characteristics of interchange mode strongly depend on the height of the magnetic hill and the strength of the magnetic shear. It is predicted theoretically that the linear growth rate of the interchange mode strongly depends on beta (gradient) and magnetic Reynolds number, S [4,5], where S is defined as τ_R/τ_A, and τ_R and τ_A are magnetic diffusion time and Alfven transit time, respectively. Previous experiments in various magnetic configurations of Heliotron-DR with low S ($\sim 10^5$) indicate that achieved beta value was limited by stability boundary of resistive interchange mode [6]. In Compact Helical System (CHS) experiments with low-S ($\sim 10^5$), no strong MHD instability was observed, whereas amplitudes of modes observed in CHS are one order higher than those observed in Large Helical Device (LHD) with high S ($\sim 10^8$) [7]. The S dependence of the mode amplitude was investigated in configurations with constant beta value under the ideally-stable condition, which shows that the saturation level of the mode is proportional to $S^{-1/3}$ and has the same dependence of the linear growth rate of the resistive interchange mode [4]. These results suggest that interchange mode can be suppressed further in reactor-relevant regime with high S. However, since the growth rate of the ideal interchange mode is independent of S, verification of the significance of the ideal stability boundary remains a major problem to be solved in helical devices. Here we focus on the effect of the mode on the confinement in the regime where the destabilization of the ideal interchange mode is predicted by linear theory.

The access to the ideal-unstable regime is possible by enhancing magnetic hill and/or by reducing the magnetic shear. The former can be realized by shifting the magnetic axis inwards, while the latter is realized by increasing the plasma aspect ratio and plasma current in co- direction. The inward shift configuration has an advantage for good transport properties because of a decrease of helical ripple, which suggests that the configuration is favorable for not only reduction of thermal transport but also confinement of alpha particle in the helical fusion reactor [8]. Therefore, to what extent MHD activity can be suppressed in the inward shifted configuration with enhanced magnetic hill should be clarified through actual experiments. The magnetic shear can be easily reduced by plasma currents flowing in co- direction. It has been predicted that the bootstrap current flows in the co- direction and is enhanced by reduction of collisionality [9], which makes the magnetic shear weaker in the reactor-relevant plasmas with low collisionality

compared to that in the high collisional plasmas of the present devices. Therefore, we should verify the actual effects of MHD activities in the ideal unstable regime for optimization of magnetic configuration for reactor design.

In this study, the effects of low-n MHD instabilities on plasma performance have been investigated in two kinds of ideal unstable regimes realized by enhancing the magnetic hill and reducing magnetic shear. The previous stability analyses of enhanced magnetic hill and reduced magnetic shear discharges show that the onset of the observed instabilities is qualitatively consistent with ideal stability boundary [10,11]. Figure 1 shows a schematic view of how to approach the ideal unstable regime. In the experiments, we changed the configurational parameters (R_{ax} and I_p) characterizing MHD instabilities based on the optimized configuration for high-beta plasma production (blue circle). The experimental setup is introduced in section 2. The experimental results in enhanced magnetic hill and weak magnetic shear configurations are described in section 3. The experiments for investigating the effect of error field on the modes also are shown in section 3. Section 4 gives discussion and summary.

2. Experimental Setup

The LHD is a heliotron device with a pair of helical coils and three pairs of poloidal coils. All coils are superconductive [12]. The typical major and minor radii are 3.6 m and 0.65 m, respectively. The available toroidal magnetic field at R_{ax}, B_t, is up to 3 T. The plasma aspect ratio, A_p, can be changed by controlling the central position of the helical coil current and it can be selected from 5.8 to 8.3 when the magnetic axis position in vacuum, R_{ax}^v, is 3.6 m. The A_p of 5.8 and R_{ax}^v of 3.6 m have been used as the standard configuration, whereas A_p of 6.6 and R_{ax}^v of 3.6 m have been applied for the high-beta operation [13]. The R_{ax}^v can be set at 3.5-4.1 m and the temporal movement of R_{ax}^v is available during a discharge by changing poloidal coil currents. The target plasmas were produced and maintained by neutral beams (NBs) and the total power is about 15 MW. The H_2 gas-puff was applied in the experiments.

In the experiments with enhanced magnetic hill, the R_{ax}^v was moved from 3.6 m to 3.5 m in 2 seconds in the configuration with B_t of 0.425 T. The A_p was set at 6.6. Figure 2 shows profiles of rotational transform and V'' in the configurations with R_{ax}^v of 3.6, 3.55 and 3.5 m, where $V'' = d^2V/d\Phi^2$, and V and Φ are the volume and the toroidal magnetic flux, respectively. The negative V'' corresponds to the magnetic hill. The pressure profile is assumed as $P = P_0(1-\rho^2)(1-\rho^8)$, where ρ is normalized minor radius. The central beta, β_0,

is 3.3 % in all investigated configurations. In the R_{ax}^{v} = 3.6 m case, the resonant surface of the m/n = 2/1 mode is located at ρ of 0.28 where the magnetic well is formed, where m and n are the poloidal mode and the toroidal mode numbers, respectively. The 2/1 resonant surface is shifted to the inward when R_{ax}^{v} is changed from 3.6 to 3.55 m, and then the surface is moved from magnetic well to magnetic hill regions. In the case of R_{ax}^{v} = 3.5 m, the resonance vanishes by increasing the central rotational transform. The m/n = 1/1 mode is predicted to be ideally stable because of relatively strong magnetic shear.

In the reduced magnetic shear experiments, the I_p was driven by two co- NBs in the configuration with R_{ax}^{v} = 3.6 m and A_p of 7.1. The $\iota/2\pi$=1 resonant surface is located at ρ of 0.7 and the magnetic shear, $1/\iota(d\iota/d\rho)$, is 1.66 in the vacuum configuration. The increases of I_p and A_p contribute to the reduction of magnetic shear and change a key instability from m/n = 2/1 to 1/1 mode because $\iota/2\pi$ = 0.5 resonant surface is vanished due to the increase in central rotational transform and $\iota/2\pi$ = 1 surface moves to the core (Fig.3). This movement decreases V'' as shown in Fig.3(b). In the experiments, it has been observed that m/n = 1/1 mode appears with I_p ramp-up and leads to minor collapse in the core [13]. The previous experiments clarified that the onset of the mode depends on beta, A_p and I_p [11].

The experiments for investigating the effect of the error field on MHD characteristics were done in the configuration R_{ax}^{v} = 3.6 m and A_p = 5.8. The $\iota/2\pi$ = 1 surface is located at ρ of 0.88, and the $1/\iota(d\iota/d\rho)$ is about 2.6 in vacuum. In LHD, the natural error field producing the m/n = 1/1 magnetic island exists, which was identified by electron beam mapping experiments [14]. The size of the island is about 23 cm in horizontally elongated cross section and the toroidal angle where the O-point is located at low field side is about -126 degrees. The resonant magnetic perturbation (RMP) system on the LHD consists of ten pairs of coils located at the top and bottom of the LHD main body. The dominant Fourier component is m/n = 1/1. The magnetic island due to the error field corresponds to that produced by RMP current of 0.1 kA when B_t = 1 T, which was applied as "reduced" error field operation described in section 3.4. The studies on the interaction between RMP field and MHD characteristics are summarized in [11, 15]

The β_0 and profiles of T_e and electron density, n_e, are measured with Thomson scattering system. The line averaged electron density is measured with FIR interferometer. The MHD modes are identified by a toroidal array with 5 magnetic probes and a helical array with 16 probes. The two saddle loop arrays each with 12 loops were used for identifying the size and spatial location of m/n = 1/1 magnetic island. [16].

3. Experimental Results

3.1 MHD Activity in Enhanced Magnetic Hill Configurations

The experiments were done in the configuration with B_t of 0.425 T. Figure 4 shows a typical discharge with real-time movement of R_{ax}^{v} inward in order to enhance the magnetic hill at $\iota/2\pi = 1/2$ surface. The R_{ax}^{v} is varied from 3.6 m to 3.5 m in 2 seconds. The central beta value starts to decrease when R_{ax}^{v} comes close to 3.53 m. The rotating $m/n = 2/1$ mode appears before the drop of the central beta, and the amplitude is increased with deceleration of the mode rotation. At 3.36 s, the mode rotation is completely stopped. Although the mode rotates and stops by turns, no recovery of the central beta is observed. Figure 5 shows the comparison of the T_e profiles before and after the stop of the rotation. The T_e profile is locally flattened at the $\iota/2\pi = 1/2$ resonance (R = 3.4 m and 3.85 m) before the stop of the rotation (3.3 s), which is caused by rotating $m/n = 2/1$ activity. After the stop of the rotation, the flattening of the profile is extended to the core region, which drops the central beta by more than 30%. It has been found that the mode can be stabilized when the R_{ax}^{v} is moved outwards during the discharge if the mode rotation is maintained.

3.2 MHD Activities in Reduced Magnetic Shear Configurations

Figure 6 shows a typical discharge in the reduced magnetic shear configuration with B_t of 1.25 T. The I_p is induced by neutral beams in order to decrease the magnetic shear in the high aspect ratio plasma configuration with low shear. While the bursts of the $m/n = 1/1$ mode appear and drop the central beta, the mode rotation slows down when the I_p exceeds about 28 kA. The minor collapse occurs after the stop of the rotation at 4.5 s, which is similar to the case of the $m/n = 2/1$ mode observed in the enhanced magnetic hill configuraiton described in section 3.1. Then the β_0 decreases by about 60%. The T_e profiles before and after the collapse are shown in Fig. 7. The rotating $m/n = 1/1$ mode forms the profile flattening around the $\iota/2\pi = 1$ resonance (3.2 m and 4.0 m). The central T_e is significantly dropped by the extension of the flattening.

3.3 Impact of MHD Modes on Central Beta Value

Figure 8 shows changes of central beta and the formation of the temperature profile flattening as a function of the mode frequency. The $m/n = 2/1$ and 1/1 activities were obtained in the enhanced magnetic hill configuration and the reduced magnetic shear configuration, respectively. In the $m/n = 2/1$ case, the flattened width normalized by the

minor radius is increased to 0.1 when the frequency is decreased to 0.4 kHz, and the central beta starts to decrease simultaneously. The m/n = 1/1 mode forms the profile flattening when the frequency falls to 0.9 kHz, and it linearly extends with the decrease in the frequency. When the frequency reaches zero, the flattened width of the temperature profile exceeds 0.5, which causes the degradation of central beta by about 60%. These results show that the mode rotation contributes to the stabilization.

3.4 Effect of Error Field on Onset of Modes

Figure 9 shows the discharges in the cases of the natural and reduced error fields. In the reduced error field case, the RMP current normalized by B_t, I_{RMP}/B_t, of 0.1 kA/T was applied and the phase is almost the same as that of the error field [14]. The $R_{ax}{}^{v}$ of 3.6 m, A_p of 5.8 and B_t of 0.9 T were selected. The white and black arrows are the onset of the m/n = 1/1 mode causing the profile flattening and the time where the mode abruptly grows, respectively. The electron density is kept at about 1×10^{19} m^{-3} in both discharges because the large beam-driven current is required to destabilize the mode in the A_p = 5.8 ratio configuration with high shear. In the discharge with the natural error field (left figure), the strong m/n = 1/1 mode appears at the time where the I_p/B_t reaches about 115 kA/T. When the I_p/B_t exceeds about 130 kA/T, the mode abruptly grows and extends the flattening region to 50% of the minor radius, which consequently drops the central electron pressure. The I_p/B_t gradually decreases after the collapse, and the w/a is decreased simultaneously. The central pressure is recovered by the stabilization of the mode in addition to the increase in the n_e. The mode is destabilized again at 5.5 s by increasing the I_p/B_t. The ion saturation currents are measured with two Langmuir probes. Both probes are located on the divertor plates at the same poloidal direction of the high field side and toroidally separated by 180 degrees. When the mode is enhanced at 4.9 s, an asymmetric structure of the ion saturation current starts to appear and extends as shown in Fig. 9 (E). This structure is due to the growth of the m/n = 1/1 mode and is in phase with the island due to the error field. After the mode is completely suppressed at 5.26 s, the asymmetric structure disappears till the mode is strongly enhanced again at 5.28 s.

In the case of the reduced error field, the mode forming the flattening appears when the I_p/B_t reaches about 118 kA/T, and it suddenly grows when I_p/B_t approaches about 133 kA/T, which are hardly different from the natural error field case. The extension of the flattening region and the drop of the central pressure are slightly larger than in the natural error field case when the collapse occurs, which may be due to the difference of the

pressure (beta) just before the collapse. The mode is stabilized by the reduction of I_p/B_t as well as in the error field case.

4. Discussion and Summary

The experiments in enhanced magnetic hill and reduced magnetic shear configurations show that the modes with finite rotation appeared firstly when the configurational parameters related to the ideal stability exceeded the thresholds, and the modes significantly grew and led to the minor collapse when the mode rotation was stopped or greatly decelerated till some threshold. The previous studies in the enhanced magnetic hill configuration clarified that the m/n = 2/1 mode is destabilized when the $\iota/2\pi = 0.5$ resonant surface moves from the magnetic well to the magnetic hill regions by the movement of the magnetic axis position to the inward [17]. Also, results of the numerical simulation show that the mode forms the flattening of the pressure profile around the resonant surface [10]. The experiments in reduced magnetic shear configurations clarified that the onset of the m/n = 1/1 mode strongly depends on beta (gradient), the plasma aspect ratio and the plasma current. The results are qualitatively consistent with theoretical prediction of low-n analysis [11]. However, the effect of the plasma flow on the modes is not included in these analyses.

The observation that the strong growth of the mode after the stop of the rotation degrades the plasma confinement is phenomenologically similar to tearing locked mode observed in tokamaks and RFPs [2, 18-20]. It has been believed that the deceleration of the tearing mode is due to the error field and the wall. However, the deceleration of the mode rotation observed in the experiments on the LHD is independent of the existence of the error field, while the mode is stopped in phase with the error field [21]. Also, it has been found in the experiments of the configurations with different plasma aspect ratios that deceleration of the mode rotation rarely depends on the distance between the resonant surface and the vacuum vessel wall. The nominal rotation of the interchange mode is quantitatively consistent with that of the sum of $\mathbf{E}\times\mathbf{B}$ and electron diamagnetic flows [22]. We consider two possibilities for the deceleration of the mode. One is due to reductions of both $\mathbf{E}\times\mathbf{B}$ and electron diamagnetic flows, which is caused by the profile flattening formed by the growth of the mode [11]. The other is due to the movement of the resonant surface to core region where the plasma flows are relatively small. This movement is due to the increase in the rotational transform caused by the plasma current.

The experimental results suggest that the significant deterioration of the plasma confinement due to the modes may be avoided if the rotation can be maintained as well as in tokamaks. Also, as shown in Fig.9, the plasma confinement can be recovered even if the plasma can return to the stable region during a discharge because of no major disruption. The effect of the plasma flow on the interchange instabilities remains an open subject. The nonlinear calculation including the plasma flow is required in order to deeply understand the physical mechanisms of the nonlinear growth of the interchange modes and the impact on the plasma confinement.

This study clarified the impact of low-*n* MHD activities on the plasma confinement in the ideal unstable regime in order to find the achievable beta regime for the helical reactor. The low-*n* instabilities deforming the plasma profile appeared when the magnetic shear was reduced or the magnetic hill was enhanced. The minor collapse decreasing the central beta by at most 60% occurred when their mode rotations were stopped. The onset of the modes is independent of the existence of the error field.

Acknowledgments

This work is supported by the NIFS under contract No NIFS14ULHH030, the Ministry of Education, Science, Sports and Culture Grant-in-Aid for Scientific Research (C) 26420858, 2014, and the JSPS-NRF-NSFC A3 Foresight Program in the field of Plasma Physics (NSFC: No.11261140328).

References

[1] ITER Physics Basis, Chapter 3: MHD stability, operational limits and disruptions 1999 Nucl.

Fusion 39 2251.

[2] Hender T. et al 2007 Nucl. Fusion 47 S128–S202.

[3] M S Chu and M Okabayashi, Plasma Phys. Control. Fusion **52** (2010) 123001

[4] Sakakibara S. et al., 2008 *Plasma Phys. Control. Fusion* **50,** 124014.

[5] Ichiguchi K. et al., 1989 Nucl. Fusion 29 2093

[6] Yanagi N. et al., 1992 Nucl. Fusion 32, 1264.

[7] Sakakibara S. et al., 2001 Nucl. Fusion **41**, 1177

[8] Yamada H. et al., 2001 *Plasma Phys. Control. Fusion* **43** A55

[9] Watanabe K.Y. et al.,1995 *Nucl. Fusion* **35** 335.

[10] Ichiguchi K. et al., *Plasma Phys. Control. Fusion* **55** (2013) 014009.

[11] Sakakibara S. et al., *Nucl. Fusion* **53** (2013) 043010.

[12] Kaneko O. et al., *Nucl. Fusion* **53** (2013) 104015.

[13] Sakakibara S. et al., *Fusion Sci. Technol.* **58** (2010) 176-185.

[14] Morisaki T. et al., *Fusion Sci. Technol.* **58** (2010) 465.

[15] Sakakibara S. et al., *Plasma Phys. Control. Fusion* 55 (2013) 014014.

[16] Sakakibara S et al., *Fusion Sci. Technol.* **58** (2010) 471.

[17] Sakakibara S et al., *Proc. 23rd IAEA Fusion Energy Conf. (Daejeon, Republic of Korea, 11-16, October, 2010*) EXS/P5-13.

[18] Shiraki D. et al., *Nucl. Fusion* **54** (2014) 033006.

[19] H van den Brand, et al., *Plasma Phys. Control. Fusion* **54** (2012) 094003,

[20] W Jin, et al., *Plasma Phys. Control. Fusion* **55** (2013) 035010.

[21] Takemura Y. et al., *Nucl. Fusion* **52** (2012) 102001.

[22] Takemura Y. et al., *Plasma Fusion Res*. **8** (2013) 1402123.

Figure Captions

Fig.1 Access to ideal unstable regime

Fig.2 Profiles of (a) rotational transform and (b) V'' in R_{ax}^{v} = 3.6, 3.55 and 3.5 m configurations.

Fig.3 Profiles of (a) rotational transform and (b) V'' in R_{ax}^{v} = 3.6 configurations with I_p = 0 and 30 kA.

Fig.4 Time evolutions of (a) central beta and preset magnetic axis position, (b) amplitude of m/n = 2/1 mode and (c) mode rotation frequency in a typical discharge in enhanced hill configuration. The amplitude of m/n = 2/1 mode was measured with magnetic probe on the vacuum vessel.

Fig.5 Electron temperature profiles at 3.3 and 3.5 s of Fig.2 discharge.

Fig.6 Time evolutions of (a) central beta and plasma current, (b) amplitude of m/n = 1/1 mode and (c) frequency in a typical discharge in reduced shear configuration.

Fig.7 Electron temperature profiles at 4.433 and 4.6 s of Fig.4 discharge.

Fig.8 Changes of (a) central beta and (b) ratio of the region of flattened temperature to minor radius as a function of normalized mode frequency.

Fig.9 Discharges in the configurations (left) with and (right) with error field reduced by RMP. Time evolutions of (A, a) plasma current, (B, b) electron density, (C, c) central electron pressure, (D, d) flattened width of T_e profile normalized by minor radius and (E, e) ion saturation currents in different toroidal sections.

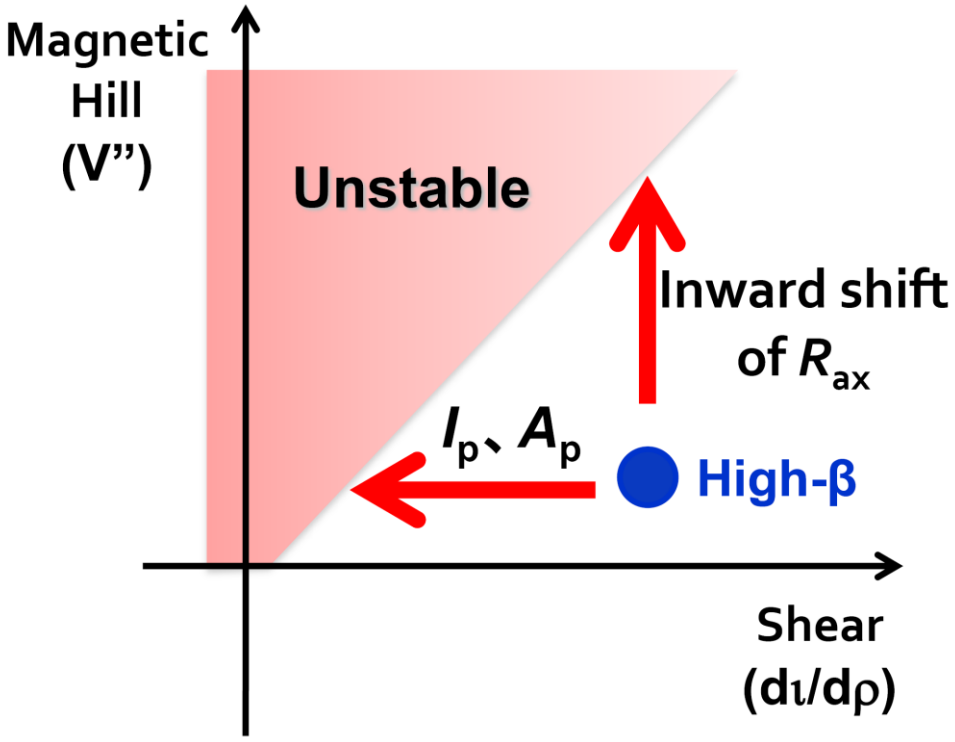

Figure 1　S.Sakakibara et al.

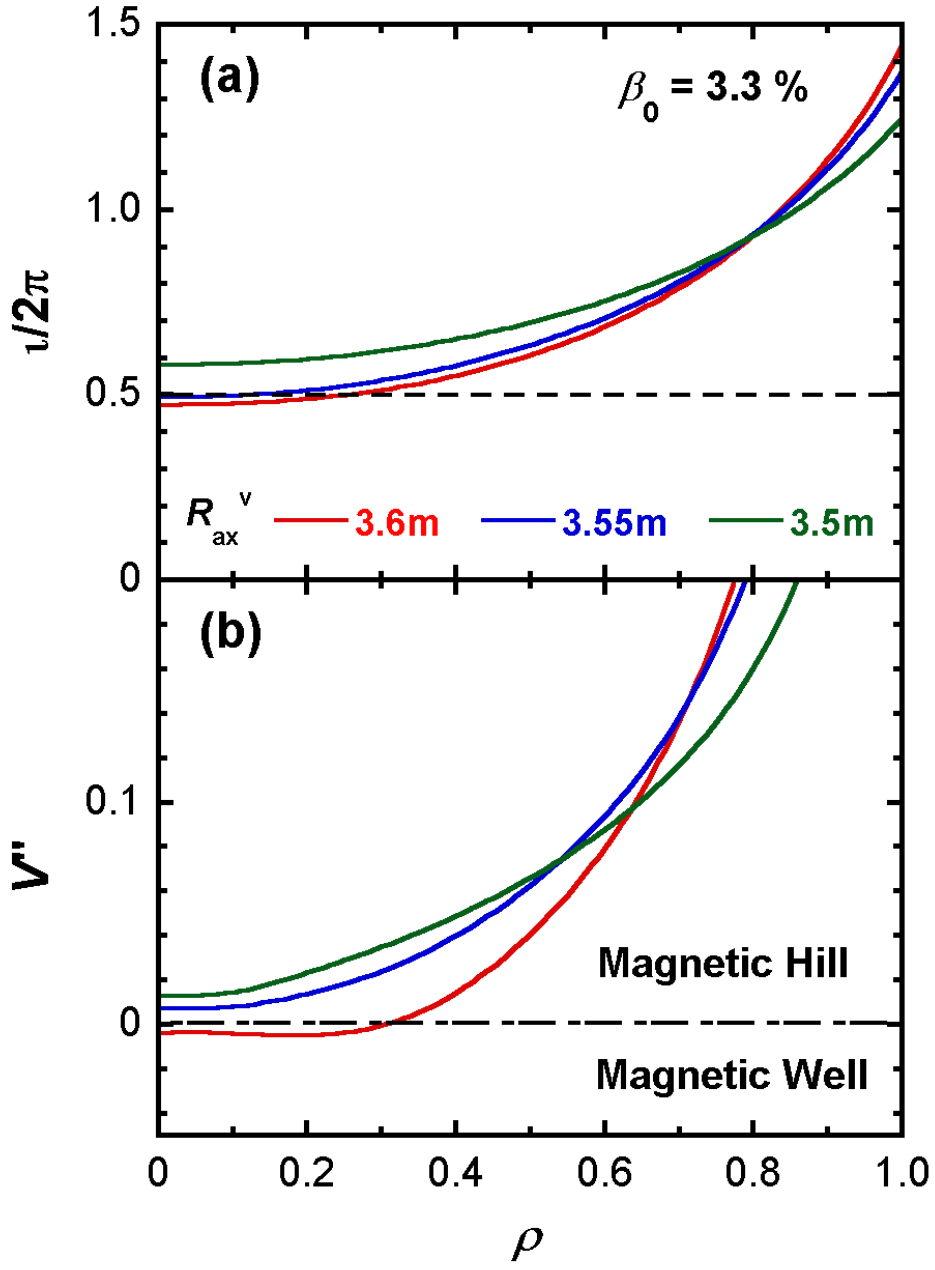

Figure 2 S.Sakakibara et al.

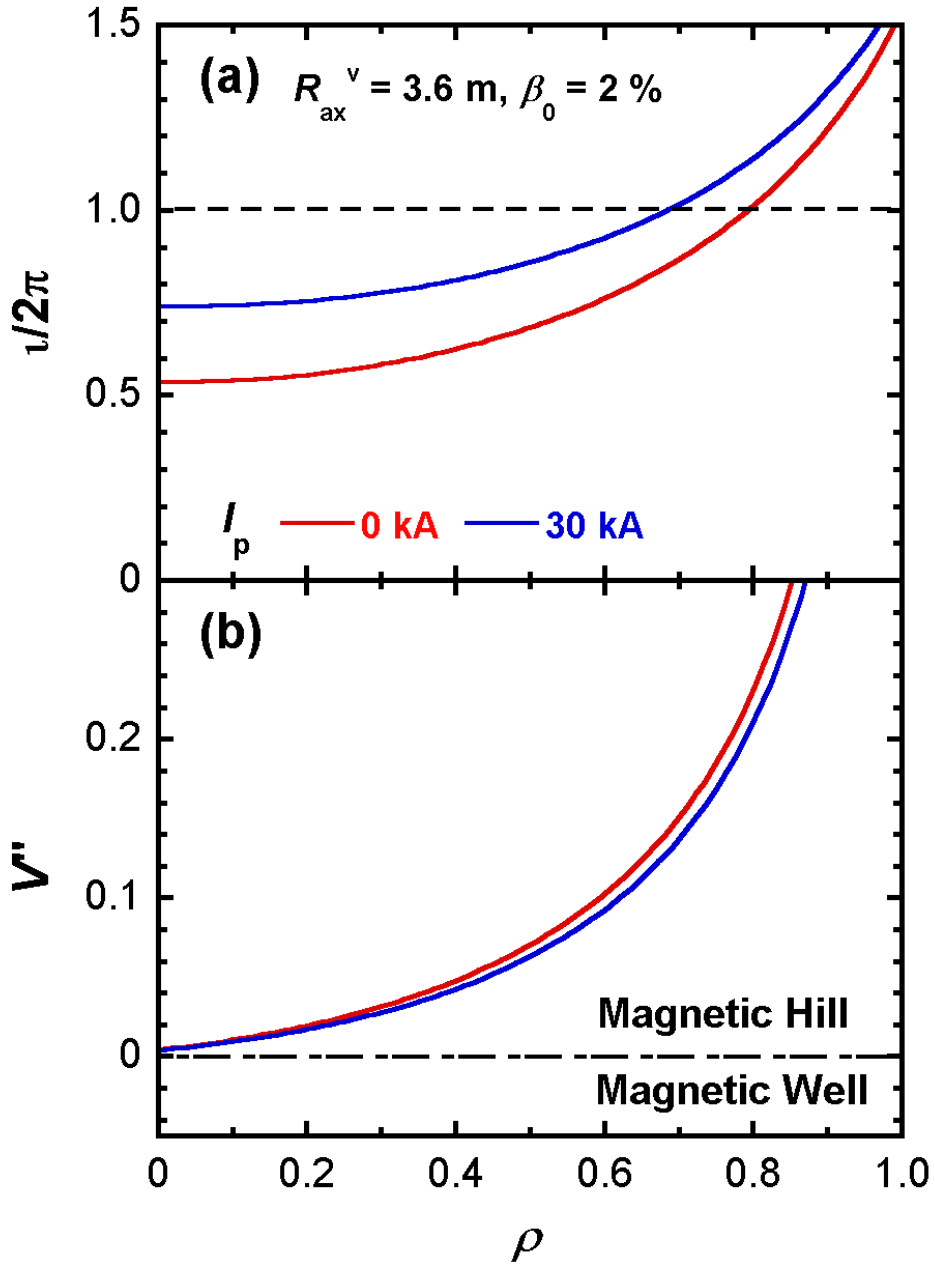

Figure 3 S.Sakakibara et al.

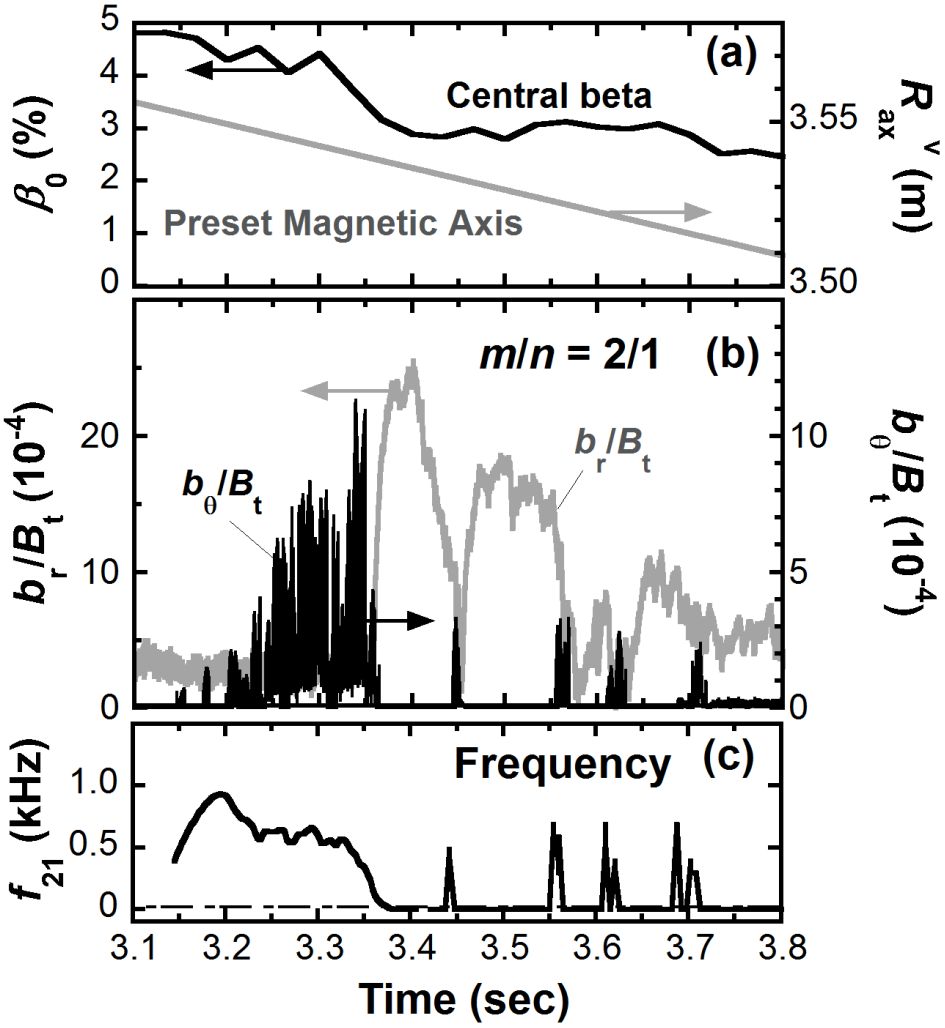

Figure 4 S.Sakakibara et al.

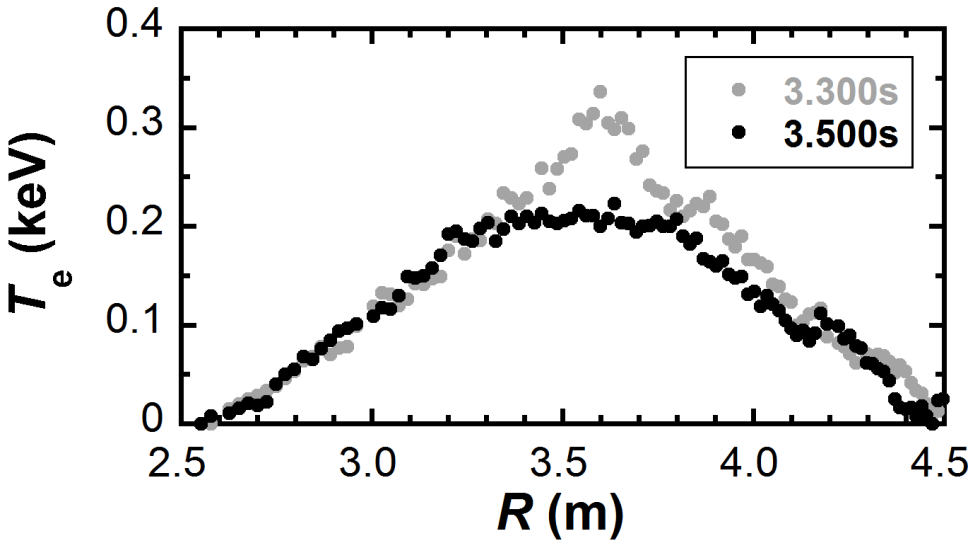

Figure 5 S.Sakakibara et al.

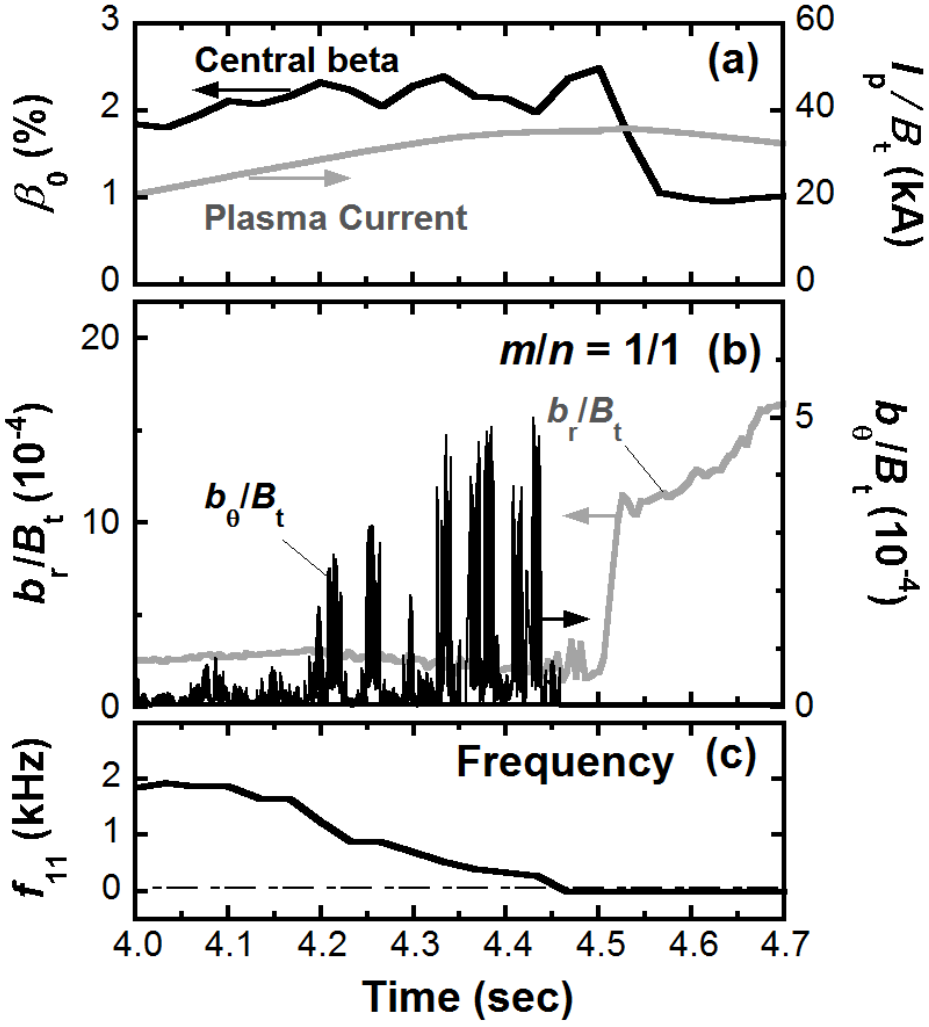

Figure 6 S.Sakakibara et al.

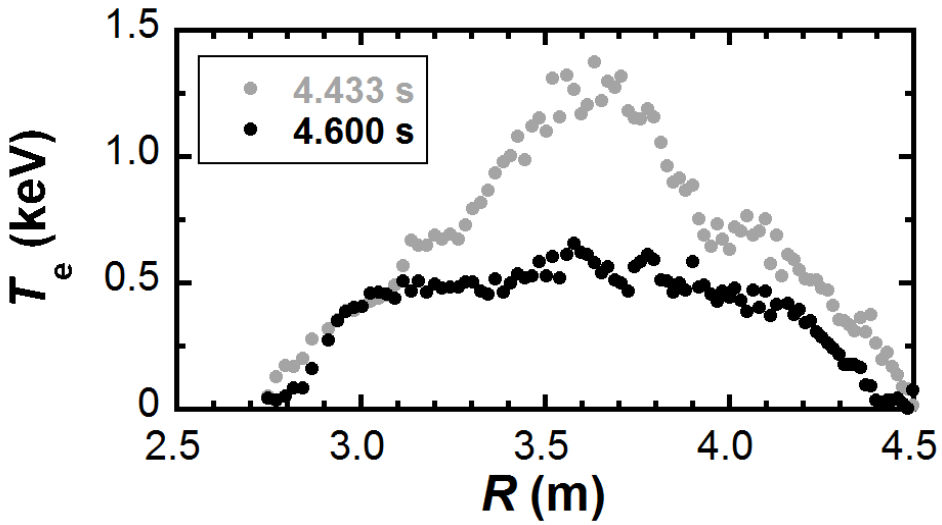

Figure 7 S.Sakakibara et al.

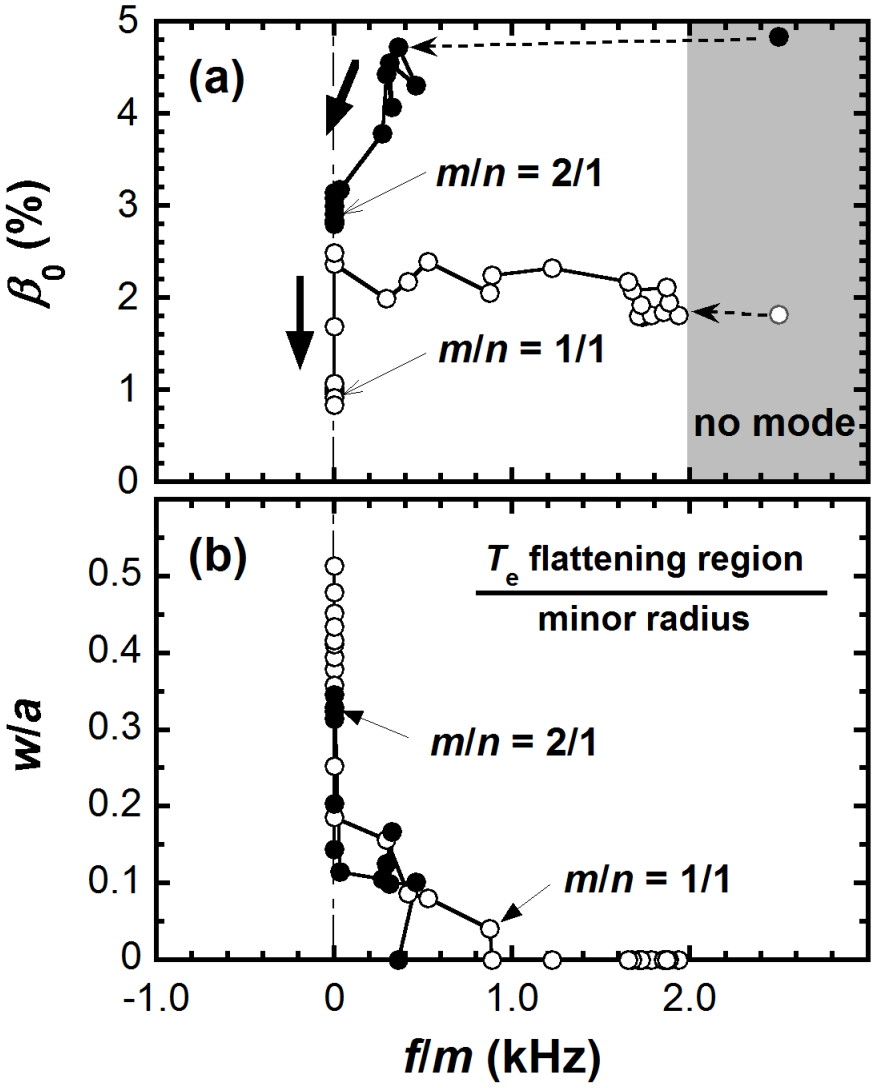

Figure 8 S.Sakakibara et al.

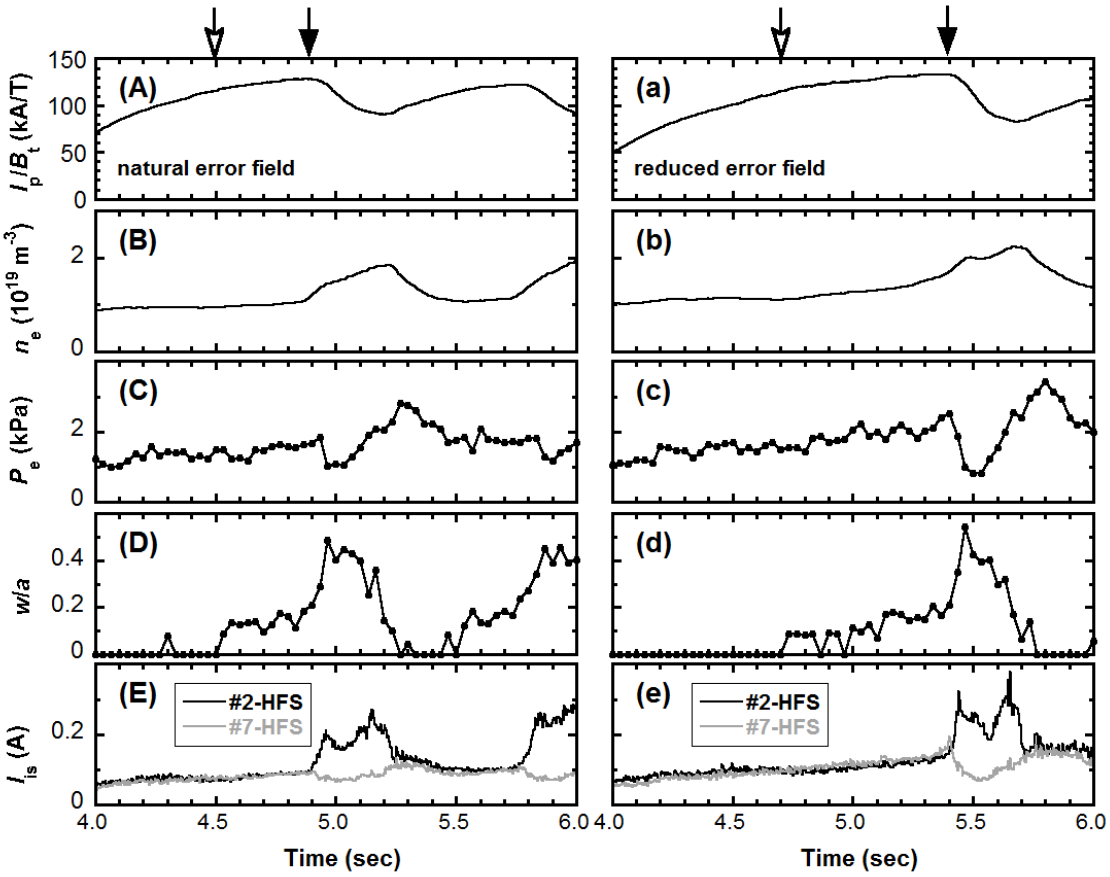

Figure 9 S.Sakakibara et al.